Local Superconductivity in Vanadium Iron Arsenide

A. S. Sefat, G. D. Nguyen, D. S. Parker, M. M. Fu, Q. Zou, H. Cao, D. Sanjeewa, Z. Gai, L. Li

We investigate vanadium-doped iron arsenides, using novel crystals, to further fundamental understanding of quantum properties in unconventional superconductors. An (average) increase in *c*-lattice parameter of the BaFe₂As₂ lattice is observed with increasing substitution of vanadium into the FeAs layers, which negates bulk superconductivity [1]. However, our combined transport and spectroscopy data find evidence for coexistence of antiferromagnetic and local superconducting regions, for the first time here in this *in-plane hole-doped iron arsenide*. This study demonstrates the complex connection between microscopic structural parameters—composition, lattice details, dopant types/sites, electronic and chemical variation, and lattice strain—and quantum bulk property emergence below a temperature.

Materials Science & Technology Division, Oak Ridge National Laboratory, Oak Ridge, TN 37831, USA
Center for Nanophase Materials Sciences, Oak Ridge National Laboratory, Oak Ridge, TN 37831, USA
Quantum Condensed Matter Division, Oak Ridge National Laboratory, Oak Ridge, TN 37831, USA

High-temperature superconductors (HTS) continue to puzzle the scientific community as their origin in iron arsenides and cuprates remains unsolved. In HTS, the superconducting state is typically produced by the suppression of an antiferromagnetic material (called a "parent") through chemical substitution (x) or applied pressure. BaFe₂As₂ (known as '122') is an iron arsenide parent [2] with a room-temperature ThCr₂Si₂-type tetragonal crystal structure; it is itinerant and only weakly correlated with a spin-density-wave (SDW) antiferromagnetic order below Néel temperature of T_N =133 K, coupled to an orthorhombic structural transition (T_N = T_s). The correlated property of 122 can be tuned by in-plane chemical substitutions of Fe using other transition metals such as T=3d (Cr, Co, Ni, Cu), 4d (Mo, Rh, Pd, Ag), or 5d (Ir, Pt, Au) in Ba(Fe_{1-x}T_x)₂As₂ [3-12]. It was found that 3d and 4d dopants belonging to a group in the periodic table produce overlapping temperature-composition (T-x) phase diagrams, emphasizing the importance of electron count [3,7,8] versus lattice size effects (i.e., 3d vs. 5d). Also, it was observed that d 'electron' dopants (e.g., Co [5]) in 122 cause superconductivity while 'hole' dopants (e.g., Cr, Mo [3,4]) do not. Such results are not well understood, especially since small doping levels of less than 5% (x<0.05) in 122s can instigate superconductivity, and it is hard to calculate how such small levels of disorder are different using a hole versus an electron dopant. But, first principles density-functional theory (DFT) calculations at 25% or 50% hole-dopants in 122 found modest covalency of d with arsenic p states [4] and some dopant-induced electronic scattering [10]. A more precise experimental recipe (for any percent doping level) was documented in a review manuscript, finding that c-axis must shrink (compared to parent) for any x, to observe 'bulk' superconductivity in an in-plane doped Ba(Fe_{1-x} T_x)₂As₂ [1]. Despite all such reports and progress in this field, it continues to be impossible to predict temperature-composition (T-x) phase diagrams and the correlated behavior in iron arsenides. In this work, we tackle doping of 122 with vanadium, and hypothesize that vanadium is less likely to carry a large moment (compared to the other hole dopants of Mn and Cr) due to its smaller number of unpaired electrons (V^{3+}, d^2) , and so Ba $(Fe_{1-x}V_x)_2As_2$ may be prone to superconductivity. We report local electronic structures in an in-plane hole-doped iron arsenide and find evidence of local superconductivity in these crystals for the first time.

Single crystals of Ba(Fe_{1-x}V_x)₂As₂ (V-122) were grown out of FeAs self-flux technique similar to ref. [13], with [001] direction perpendicular to the plates. The chemical composition of the crystals was measured with a Hitachi S3400 scanning electron microscope and use of energy-dispersive X-ray spectroscopy (EDS). The structures were identified as tetragonal ThCr₂Si₂ type (*I4/mmm*, Z=2) at room temperature, and lattice parameters upon doping were refined using X'Pert HighScore by collecting data on an X'Pert PRO MPD X-ray powder diffractometer (See **Table S1** in **S**upplementary section). **Fig. 1a** plots *a*- and *c*-lattice parameters as a function of V concentration. With V doping, the *a*-lattice decreases while the *c*-lattice parameter increases. In the hole doped Cr-122 both *a* and *c* increase, while in Mo-122 *a*-lattice barely changes while *c* expands. For x=0.05 doping in Ba(Fe_{1-x}T_x)₂As₂, the overall cell volume increases by 0.3% for T=Cr and 0.5% for Mo [3], while it only expands by ~0.1% for V. All the 122 in-plane hole-doped iron arsenides expand their *c* lattice.

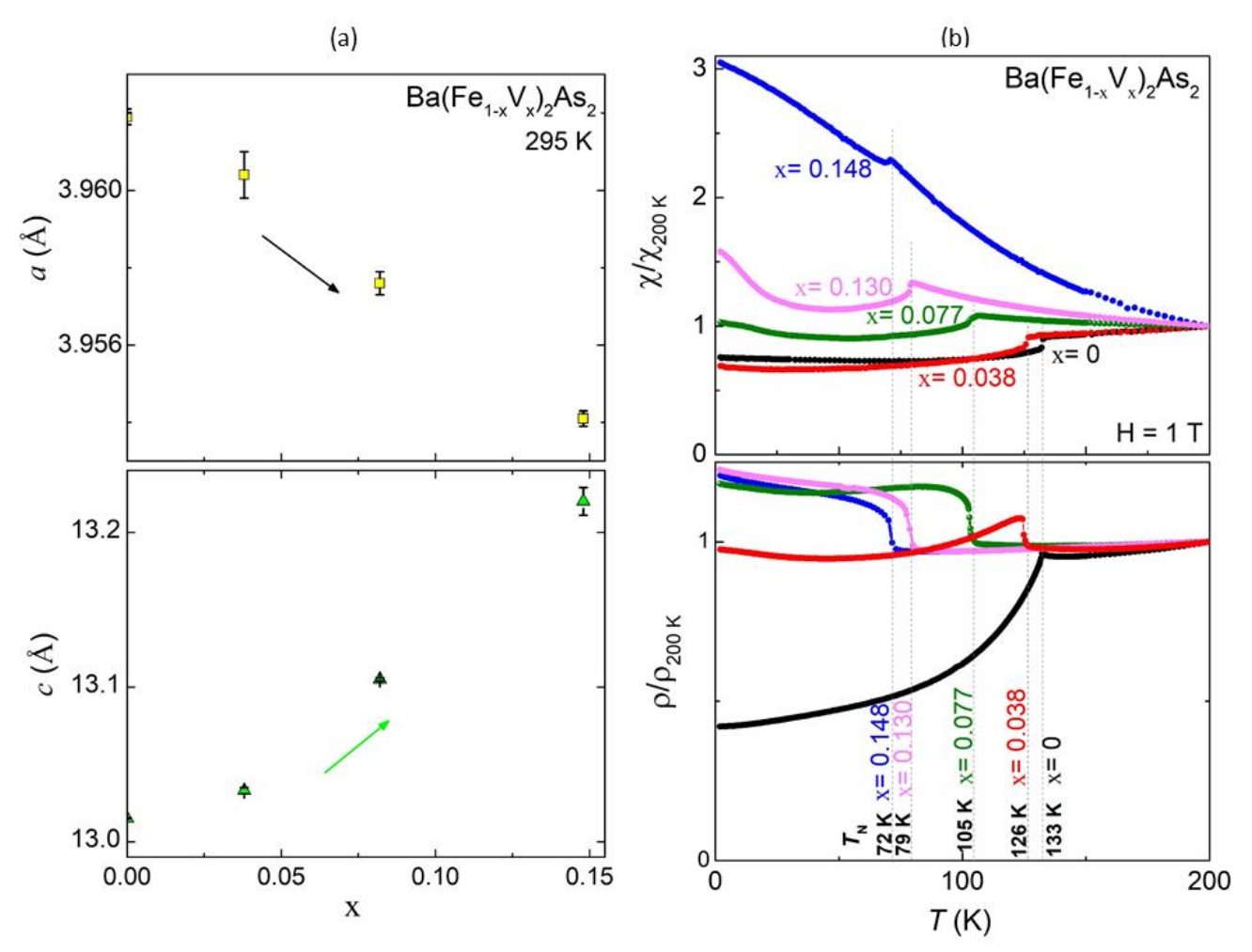


FIG. 1: Ba(Fe_{1-x}V_x)₂As₂: (a) Room-temperature tetragonal *a*- and *c*-lattice parameters for the range of possible vanadium chemical substitutions (x). (b) Temperature-dependent magnetic susceptibility χ (top) and resistivity ρ (bottom), normalized to 200 K data. Magnetization is measured in zero-field-cooling after applying 1 Tesla along *ab*-axis; resistance is measured in the *ab*-plane. Anomalies for Néel ordering temperature (T_N) match in χ and ρ . For x=0.038 T_N =128 K, and some crystals give an additional feature at T^* =20 K (see **Fig. 2a**).

Magnetization and electrical resistance data for Ba(Fe_{1-x}V_x)₂As₂ were collected using Quantum Design's magnetic and physical property measurement systems, respectively. For the temperature-sweep magnetization experiments, each sample was cooled to 1.8 K in a zero field and data were collected by warming from 1.8 to ~300 K in 1 Tesla along the *ab*-crystallographic direction. The data are presented in the form of χ/χ_{200K} for all x, to show changes to magnetic transitions (**Fig. 1b**, top). For the parent and as expected, χ decreases with lowering temperature and drops abruptly below T_N = T_s =133 K. For x = 0.038, 0.077, 0.130, the χ feature is the same although the transition temperatures are reduced with x; for x=0.148, the anomaly is lowest and χ increases below. The electrical resistance measurements were performed in the *ab*-plane of the crystals, by attaching platinum leads using Dupont 4929 silver paste. The values of resistivity did not change much between compositions, being on the order of a few mΩ cm, with absolute values carrying errors

due to geometry factors; data is presented in the form of ρ/ρ_{200K} (**Fig. 1b**, bottom). Electrical resistivity for x=0 and 0.038 diminishes with decreasing temperature falling rapidly below 133 K associated with T_N and T_s ; the crystals from x=0.038 batch may show an additional ρ downturn below T^* =20 K (see **Fig. 2a**). The $\rho(T)$ for x \geq 0.077 first decreases from room temperature, then has a sharp upturn below. The upturn in ρ reflects the loss of carriers as a partial SDW gap opens at T_N , and for temperatures below T_N , the increase in the mobility of the remaining carriers is probably not enough to overcome the lower carrier concentration and ρ continues to increase. For Ba(Fe_{1-x}V_x)₂As₂, the inferred Néel ordering temperatures estimated from anomalies in $\chi(T)$ and $\rho(T)$ are T_N =133 K for x=0, T_N =128 K for x=0.038, T_N =105 K for x=0.077, T_N =105 K for x=0.130, and T_N =72 K for x=0.148. For vanadium doping of x=0.130, neutron diffraction confirms that T_N = T_S =79 K (see **Fig. S1**).

To reveal the correlation between the nanoscale structure with the bulk chemical, electronic, and magnetic behavior observed above, we performed scanning tunneling microscopy/spectroscopy (STM/S) measurement on Ba(Fe_{1-x}V_x)₂As₂ with x=0.038. The resistance data on the piece measured using STM/S is shown in Fig. 2a; in addition to an anomaly at T_N , there is a small downturn in resistance below $T^*=20$ K that is reduced to 13 K upon application of 8 Tesla magnetic field. Regarding this mysterious downturn in resistance in a sample of Ba(Fe_{1-x}V_x)₂As₂, the literature shows other lightly hole-doped Cr [4] and Mo [3] 122 crystals having such p drops below T^* without reaching zero. Such T^* transition was found to be weakly x dependent, with no structural/magnetic transitions detected in neutrons, and was argued to result from nanoscale chemical phase segregation or even an impurity inclusion [4]. Since it is evident in all lightly holedoped crystals, we presume that it has an intrinsic origin and investigate the local electronic structure for the first time here. The sample was cleaved in situ at liquid nitrogen temperature. A large scale STM image is shown in Fig. 2b, which presents large terraces and a step with height of ~0.7 nm, close to half the c-axis lattice parameter of 122. Fig. 2c shows a typical atomic resolution STM image on the surface area with 2×1 surface reconstruction. The corresponding superconducting gap map (Fig. 2d) at the temperature of 5 K is calculated from the current imaging tunneling spectroscopy (CITS), similar with those reported for in-plane electron-doped iron arsenides [14]. Although majority of the crystal does not show a gap feature, some potentially localized superconducting areas are detected mostly near domain boundaries (marked dashed blue lines) and some bright spots on the surface which are due to sub-layer defects. The superconducting regions are localized, in the range of one unit-cell up to a few nanometers. Fig. 2e present line spectra across such a superconducting area (Fig. 2c, black arrow). The red curves in the superconducting phase area clearly show a superconducting-like gap with the requisite coherence peaks. A few unit cells away from this area, the dI/dV spectra show pseudo-gap characteristics (green curves) and then exhibit normal metallic phase behavior (black curves). Fig. 2f shows the temperature evolution of the dI/dV spectra at the exact crystal location as the likely superconducting phase area (Fig. 2c, blue dot). With increasing temperature, this gap is suppressed and eventually disappears above 20 K. It is important to note that this 20 K gap suppression temperature is consistent with the downward transition temperature from our bulk resistivity measurements (Fig. 2a, inset), suggesting a common origin for these distinct features.

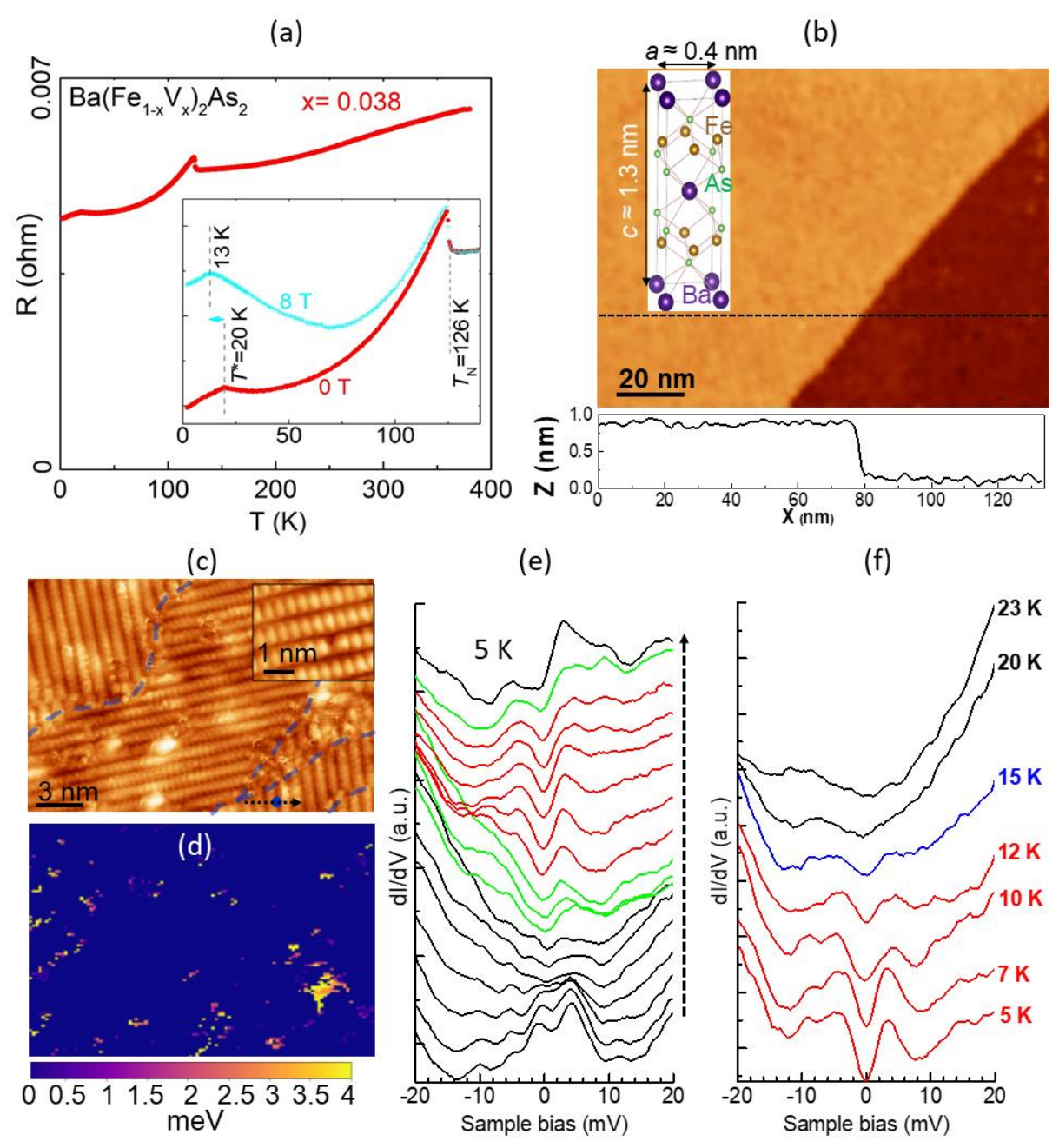


FIG. 2. For Ba(Fe_{1-x}V_x)₂As₂ crystal with x=0.038. (a) Temperature dependent resistance data on a piece, with an anomaly associated with T_N =126 K magnetic ordering, and another transition at T^* =20 K that is field dependent. (b) Large-scale STM topographic image of (V_S = -10 mV, I_t = 100 pA). (c) Short-scale STM topographic image on the surface with **2** × **1** surface reconstruction (V_S = -20 mV, I_t = 200 pA), where blue dashed line marks the domain boundary; inset is atomic resolution image (V_S = -3 mV, I_t = 200 pA). (d) Superconducting gap map extracted from CITS measurement at 5 K. (e) dI/dV line spectra taken across a superconducting phase area marked by the black dashed arrow in (c); spatial distance between each curve is 0.21 nm (red and green curves label the superconducting and pseudogap phase spectra, respectively). (f) Temperature dependent dI/dV spectra taken at the same location of blue dot in (c), showing the transition temperature at ~ 20 K; vertical offsets are applied to the spectra for clarity.

In addition, there are several other pieces of information that taken together comprise a strong case for local superconductivity in this in-plane hole-doped iron arsenide. Firstly, we note from Fig. 2f that the gap size Δ at the low temperature of 5 K is approximately 4 meV, or 2.3 times the 20 K T^* value. This is in the range for moderate-to-strong coupling superconductivity, given the BCS weak-coupling s-wave ΔT_c value of 1.76. While some form of density-wave order [15] could show a similar ΔT_c value, there is one additional fact that argues strongly for the likelihood of local superconductivity here. As shown in the inset of Fig. 2a, the resistivity feature at 20 K drops to a temperature of 13 K under a field of 8 T. While it is unlikely that a spin or charge-density-wave would show such a change in temperature, we can even make a stronger quantitative statement. The Pauli-limited upper critical field H_{c2} , in the BCS approximation, for a 20 K superconductor would be approximately 36 T [16]. Assuming a linearity in H_{c2} , one would then expect an 8 T field to reduce the resistivity feature temperature by approximately 5 K, in general agreement with the 7 K reduction we see. Moreover, there is a notable correspondence (most likely not coincidental) between these results and our previous results [5] on electron-doped BaFe₂As₂: In the work on cobalt-doped BaFe₂As₂ we observed a superconducting phase with $T_c = 21$ K for $x_{Co} =$ 0.1. Note that, in terms of charge count, this is virtually an equivalent doping (of opposite sign) to our $x_V=0.037$ doping, as V has three fewer valence electrons than Fe, and that the T_c observed there is nearly identical to our T^* here. Furthermore, in that work we observed, under application of the same 8 T field, a very similar reduction in T_c (5 K) to our 7 K reduction in T^* here. Taken together, all these notes suggest that what we are observing is in fact a local superconductivity.

The local superconducting areas near domain boundaries might share the same origin as in the recent proposals in iron arsenide superconductors, in which superconducting states are induced by local strains or interfaces [17-21]. In this case, however, this state is partly induced by vanadium doping. In parallel with observing the local superconducting phase, the crystal of Ba(Fe_{1-x}V_x)₂As₂ with x=0.038 also demonstrates SDW when scanning at other crystal regions (see **Fig. S2**), similar to other iron asenides [22]. Hence, non-percolative local superconductivity in V-122 seems to coexist with antiferromagnetism, which is first documented for a hole-doped iron arsenide here. Given the local superconductivity around x = 0.038 for V, it is plausible to argue that there is a nanoscale phase separation associated with the V substitution, with some small regions exhibiting the local superconductivity described previously and the larger fraction maintaining the antiferromagnetic character. In fact, first-principles calculations for vanadium show evidence for stronger scattering compared to cobalt dopants (see **Fig. S3**), which is likely strongest in the physical vicinity of a V dopant atom and weaker at greater distance. As the doping level is so small (<4%), this may show variation in bulk ρ properties in different pieces of as-grown crystals.

A major unanswered question, however, is the local relationship of the vanadium with the apparent superconductivity. It is tempting to associate the few percent reduction in ρ in the superconducting phase with the few percent (x=0.038) of V present in the crystal and thereby correlate the location of the V atom with the local superconductivity. However, the STM results do not confirm this and in addition, in such a scenario the local environment would be highly overdoped, containing an electron count (per cell) of order unity less than the majority phase. This is unlikely to show a superconductivity with the $T^*_{c}\sim20$ K that we observe. It is more likely that a combination of charge doping, strain, and reduced scattering in the vicinity of the grain boundaries allows a local superconductivity to emerge in this in-plane hole-doped iron arsenide.

We report synthesis and bulk properties of novel vanadium-doped BaFe₂As₂ crystals, and describe electronic structures using density-functional-theory and local-scale spectroscopy. The increase in c-lattice parameters of the 122 lattice with increasing V dopants is observed, which negates 'bulk' superconductivity [1]. In fact, the antiferromagnetic transition of 122 (T_N =133 K) is suppressed to T_N =72 K for Ba(Fe_{1-x}V_x)₂As₂ with x=0.148, with non-zero resistivity and no Meissner effect down to 2 K. However, for low x (<4%) there is evidence of a coexisting antiferromagnetic and nanometer superconducting regions that is found in spectroscopy and is encouraged by first principles calculations. Such local superconductivity in an iron arsenide may explain the lack of bulk superconductivity at higher x for any in-plane hole-dopants (e.g., V, Cr, Mo, Mn) and the potential for creating percolative superconducting path in any 122s.

This manuscript has been authored by UT-Battelle, LLC under Contract No. DE-AC05-00OR22725 with the U.S. Department of Energy. The United States Government retains and the publisher, by accepting the article for publication, acknowledges that the United States Government retains a non-exclusive, paid-up, irrevocable, world-wide license to publish or reproduce the published form of this manuscript, or allow others to do so, for United States Government purposes. The Department of Energy will provide public access to these results of federally sponsored research in accordance with the DOE Public Access Plan.

The research is supported by the U.S. Department of Energy (DOE), Office of Science, Basic Energy Sciences (BES), Materials Science and Engineering Division.

- [1] L. M. N. Konzen, and A. S. Sefat, J. Phys.: Condens. Matter 29 (2017), 083001.
- [2] M. Rotter, M. Tegel, D. Johrendt, I. Schellenberg, W. Hermes, and R. Pottgen, Phys. Rev. B 78, 020503 (2008).
- [3] A. S. Sefat, K. Marty, A. D. Christianson, B. Saparov, M. A. McGuire, M. D. Lumsden, W. Tian, and B. C. Sales, Phys. Rev. B 85, 024503 (2012).
- [4] A. S. Sefat, D. J. Singh, L. H. VanBebber, Y. Mozharivskyj, M. A. McGuire, R. Jin, B. C. Sales, V. Keppens, and D. Mandrus, Phys. Rev. B **79**, 224524 (2009).
- [5] A. S. Sefat, R. Jin, M. A. McGuire, B. C. Sales, D. J. Singh, and D. Mandrus, Phys. Rev. Lett. **101**, 117004 (2008).
- [6] N. Ni, and S. L Bud'ko, Mater. Research Bull. 36, 620 (2011).
- [7] K. Marty, A. D. Christianson, C. H. Wang, M. Matsuda, H. Cao, L. H. VanBebber, J. L. Zarestky, D. J. Singh, A. S. Sefat, and M. D. Lumsden, Phys. Rev. B 83, 060509(R) (2011).
- [8] N. Ni, A. Thaler, A. Kracher, J. Q. Yan, S. L Bud'ko, and P. C. Canfield, Phys. Rev. B **80**, 024511 (2009).
- [9] L. Li, H. Cao, D. S. Parker, S. J. Kuhn, and A. S. Sefat, Phys. Rev. B 94, 134510 (2016).
- [10] X. Zhu, F. Han, G. Mu, P. Cheng, J. Tang, J. Ju, K. Tanigaki, and H.-H. Wen, Phys. Rev. B **81**, 104525 (2010).
- [11] X. L. Wang, H. Y. Shi, X. W. Yan, Y. C. Yuan, Z.-Y. Lu, X. Q. Wang, and T.-S. Zhao, Appl. Phys. Lett. **96**, 12507 (2010).
- [12] L. Li, H. Cao, M. A. McGuire, J. S. Kim, G.R. Stewart, and A. S. Sefat, Phys. Rev. B **92**, 094504 (2015).
- [13] A. S. Sefat, Current Opinion Solid State Mater. Sci. 17, 59 (2013).
- [14] Q. Zou, Z. M. Wu, M. M. Fu, C. M. Zhang, S. Rajput, Y. P. Wu, L. Li, D. S. Parker, J. Kang, A. S. Sefat, and Z. Gai, Nano Lett. **17**, 1642 (2017).
- [15] G. Gruner. Density waves in solids. CRC Press (2018).

- [16] S. Khim, J. W. Kim, E. S. Choi, Y. Bang, M. Nohara, H. Takagi, and K. H. Kim. *Phys. Rev. B* **81**, 184511 (2010).
- [17] S. Saha, N. Butch, K. Kirshenbaum, J. Paglione, and P. Zavalij, Phys. Rev. Lett. **103**, 037005 (2009).
- [18] K. Zhao, B. Lv, L. Deng, S.-Y. Huyan, Y.-Y. Xue, and C.-W. Chu, Proc. Natl. Acad. Sci. 113, 12968 (2016).
- [19] J. Engelmann, V. Grinenko, P. Chekhonin, W. Skrotzki, D.V. Efremov, S. Oswald, K. Iida, R. Hühne, J. Hänisch, M. Hoffmann, F. Kurth, L. Schultz, and B. Holzapfel, Nature Comm. **4**, 2877 (2013).
- [20] H. Xiao, T. Hu, A.P. Dioguardi, N. Roberts-Warren, A.C. Shockley, J. Crocker, D.M. Nisson, Z. Viskadourakis, X. Tee, I. Radulov, C. C. Almasan, N. J. Curro, and C. Panagopoulos, Phys. Rev. B **85**, 024530 (2012).
- [21] T. Ozaki, L. Wu, C. Zhang, J. Jaroszynski, W. Si, J. Zhou, Y. Zhu, and Q. Li, Nature Comm. 7, 13036 (2016).
- [22] J. E. Hoffman, Rep. Prog. Phys. 74, 124513 (2011).

Supplemental Material for

Local Superconductivity in Vanadium Iron Arsenide

A. S. Sefat, G. D. Nguyen, D. S. Parker, M. M. Fu, Q. Zou, H. Cao, D. Sanjeewa, Z. Gai, L. Li

In this Supplement, we provide additional information regarding: (i) growth and structure, (ii) local magnetic structure, (iii) density of states.

GROWTH AND STRUCTURE

To produce a range of dopant concentrations of Ba(Fe_{1-x}V_x)₂As₂ crystals, small barium chunks, V powder (VAs powder for getting uniform sample with high doping level), and FeAs powder were combined according to various loading ratios of V(or VAs): FeAs in alumina crucibles. A second catch crucible containing quartz wool was placed on top of each growth alumina crucible, and both were sealed inside a silica tube under ~1/3 atm argon gas. Each reaction was heated for ~24 h at 1180 °C, and then cooled at a rate of 2°C/h, followed by a decanting of the flux around 1090 °C [S1]. The several-millimeter sized crystals formed with the [001] direction perpendicular to the plates. The chemical composition of the crystals was measured with a Hitachi S3400 scanning electron microscope operating at 20 kV and use of energy-dispersive x-ray spectroscopy (EDS). For finding the level of x, at least three spots (~90 µm diameter each) were averaged on crystalline pieces in each as-grown batch. The measured EDS values are reported as vanadium (x) in **Table** S1, and thermodynamic and transport bulk properties are denoted by x. Phase purity and lattice parameters upon doping were checked by collecting data on an X'Pert PRO MPD X-ray powder diffractometer in the 5–90° 2θ range. At room temperature, the structures were identified as the tetragonal ThCr₂Si₂ structure type (I4/mmm, Z=2). The air and moisture stability of the crystals were confirmed by rechecking the diffraction scan of a sample left overnight. Lattice parameters were determined from full-pattern LeBail refinements using X'Pert HighScore, listed in **Table S1**.

Neutron diffraction experiments were performed at the High Flux Isotope Reactor at ORNL, using HB-3 triple-axis spectrometers, on a crystal of Ba(Fe_{1-x}V_x)₂As₂ with x=0.130 in order to confirm magnetism and coupling of magnetic and structural transitions inferred from properties at ~79 K. Results are shown in **Fig. S1**, also featuring data of the parent as comparison. The ordering temperature for the magnetic transition from non-magnetic state to SDW order [122 with known propagation vector in Tetragonal cell (½ ½ 1)_T] is determined by the intensity of the strongest magnetic reflection (½ ½ 5)_T. For tracking the tetragonal-to-orthorhombic transition, the intensity of the (2 2 0)_T nuclear peak was measured with warming; the intensity increase below the T_s is due to a reduced extinction effect, caused by the structural transition from tetragonal to split into (4 0 0)_O and (0 4 0)_O reflections (O refers to orthorhombic vector basis), resulting in a significant change in the peak intensity at the transition. Hence for x=0.130, neutron diffraction confirms that T_N = T_s =79 K.

 ¹ Materials Science & Technology Division, Oak Ridge National Laboratory, Oak Ridge, TN 37831, USA
² Center for Nanophase Materials Sciences, Oak Ridge National Laboratory, Oak Ridge, TN 37831, USA
³ Quantum Condensed Matter Division, Oak Ridge National Laboratory, Oak Ridge, TN 37831, USA

TABLE S1. A few of flux grown Ba(Fe_{1-x} V_x)₂As₂ crystals: the resulting vanadium concentration (x) and the refined lattice parameters.

V (x)	<i>a</i> -lattice parameter (Å)	c-lattice parameter (Å)
0	3.9619(2)	13.0151(2)
0.038	3.9604(6)	13.033(2)
0.082	3.9576(3)	13.105(1)
0.148	3.9541(2)	13.220(9)

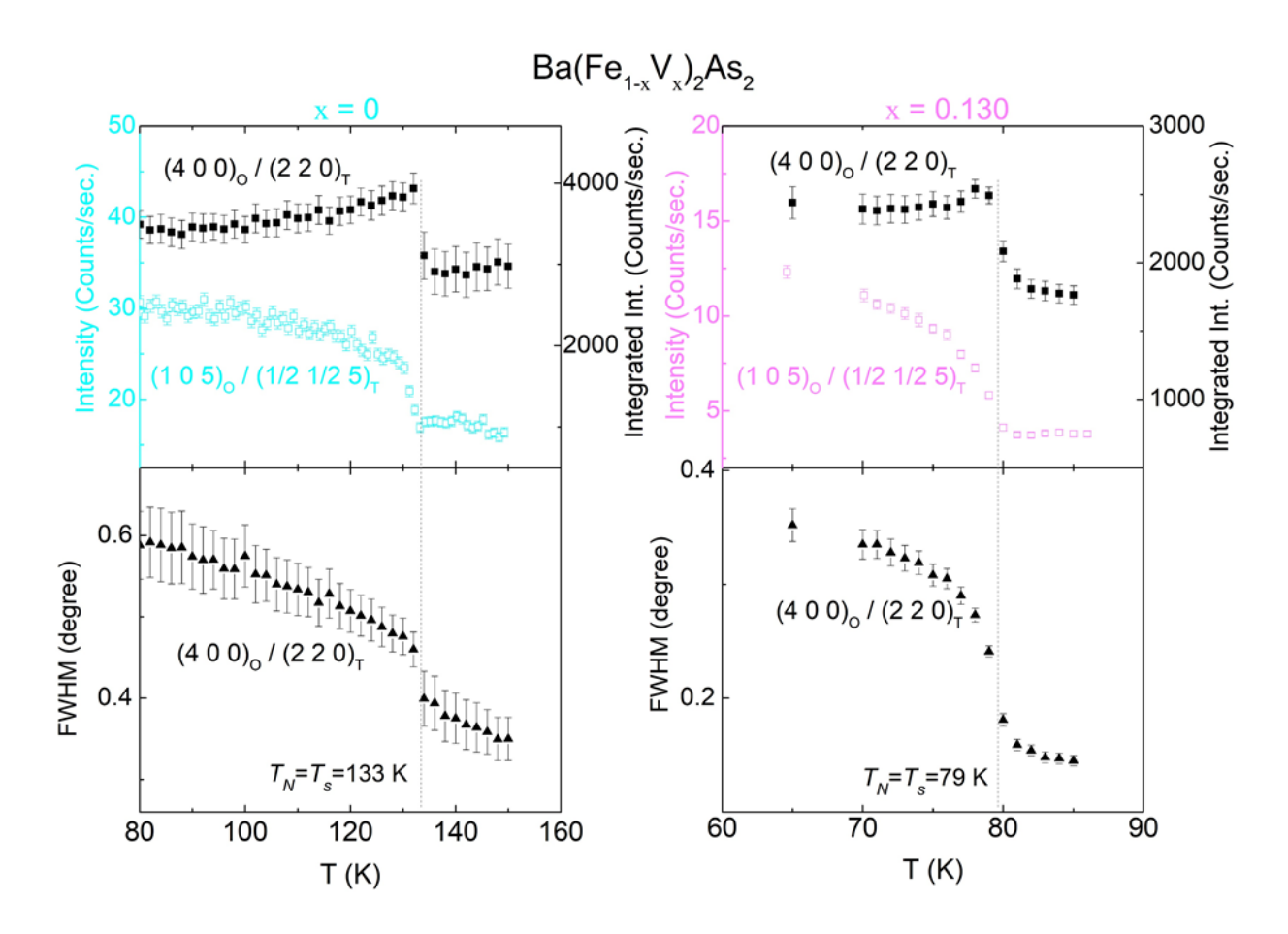


FIGURE S1. For Ba(Fe_{1-x}V_x)₂As₂ crystals, neutron diffraction results for x=0 (left) compared to x=0.130 (right). Top panels: integrated intensity of the nuclear peak (4 0 0)_O/(2 2 0)_T and peak intensity of magnetic peak (1 0 5)_O/(½½ ½ 5)_T. Bottom panels: full width at half maximum values of peaks. The dashed lines mark the overlapped structural and magnetic transition for both samples at $T_N=T_s$.

LOCAL MAGNETIC STRUCTURE

Fig. S2a, b show an STM topographic image and dI/dV tunneling conductance map of a surface area of Ba(Fe_{1-x}V_x)₂As₂ crystal with x=0.038 that demonstrate non-superconducting states. The Fast Fourier transform (FFT) of the conductance map reveals the *q*-space structure through quasiparticle interference (QPI) patterns induced by scattering of electronic states with defects. The QPI disclose the C₂ symmetry of the q-space structure which is similar to QPI in the SDW state found in other iron arsenides [S2]. Four white circles in Fig. S2c mark the wave vectors corresponding to the nearly square atomic lattice. There are two prominent scattering wave vectors q₁ and q₂ aligned along the Fe-Fe bond direction which is approximately 45° with the orthorhombic *a*- and *b*-axes. The scattering wave vector q₁≈2 π /8 $a_{\text{Fe-Fe}}$ ($a_{\text{Fe-Fe}}$ = a_0 /√2) corresponds to a periodicity of ~ 8 $a_{\text{Fe-Fe}}$ in real space. In addition, we observe another scattering wave vector q₂≈2 π /4 $a_{\text{Fe-Fe}}$. Based on the theoretical simulations for QPI in iron arsenides [S3, S4], the wave vector q₁ originates from the intrapocket scattering in a center ellipse-like hole pocket while q₂ comes from the interpocket scattering between small electron pockets beside it. Hence, non-percolative local superconductivity in the hole-doped V-122 seems to coexist with antiferromagnetism, which is evident here for the first time.

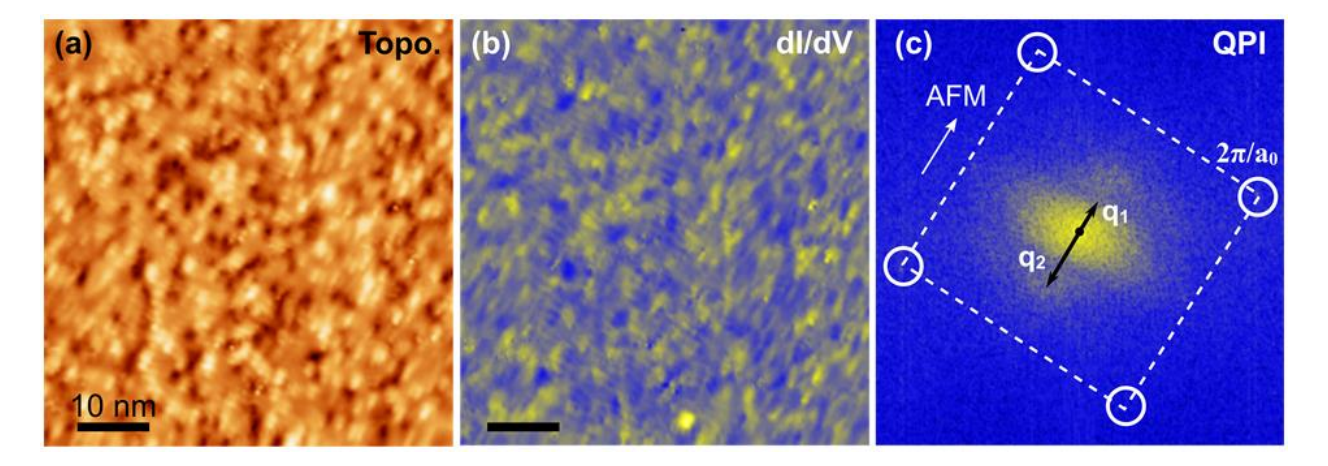


FIGURE S2: For Ba(Fe_{1-x}V_x)₂As₂ crystal with x=0.038. (a), (b) STM topographic image and dI/dV tunneling conductance map on the surface area with non-superconducting phase ($V_S = -5$ mV, $I_t = 200$ pA, $V_{ac} = 0.5$ mV, f = 973 Hz, T = 5 K). (c) FFT of conductance map in (b) which demonstrate anisotropic QPI with C₂ symmetry.

DENSITY OF STATES

The DOS for cobalt versus vanadium dopants into BaFe₂As₂ are shown in **Fig. S3**. These calculations were performed using the orthorhombic lattice parameters for 122, with one of the eight Fe substituted by the respective dopant, in a non-magnetic state. As before, we use the local density approximation and experimental arsenic height in these calculations [S5-S7]. Comparing cobalt to vanadium, cobalt is suggested for robust superconductivity as its DOS mimics that of the overall crystal matrix, both in shape and proportion, resulting in minimal scattering for substituting in 122. For vanadium, there is an absolute maximum approximately 1 eV above E_F and some 1 to 2 eV above the corresponding maxima in the total DOS curve. This difference in shape indicates

the likelihood of some scattering compared to that of Co, but it not as extreme as in Ag doping [S5]. Speaking from a real-space perspective, such scattering is likely stronger in the physical vicinity of a V dopant atom and would be expected to be weaker at greater distance.

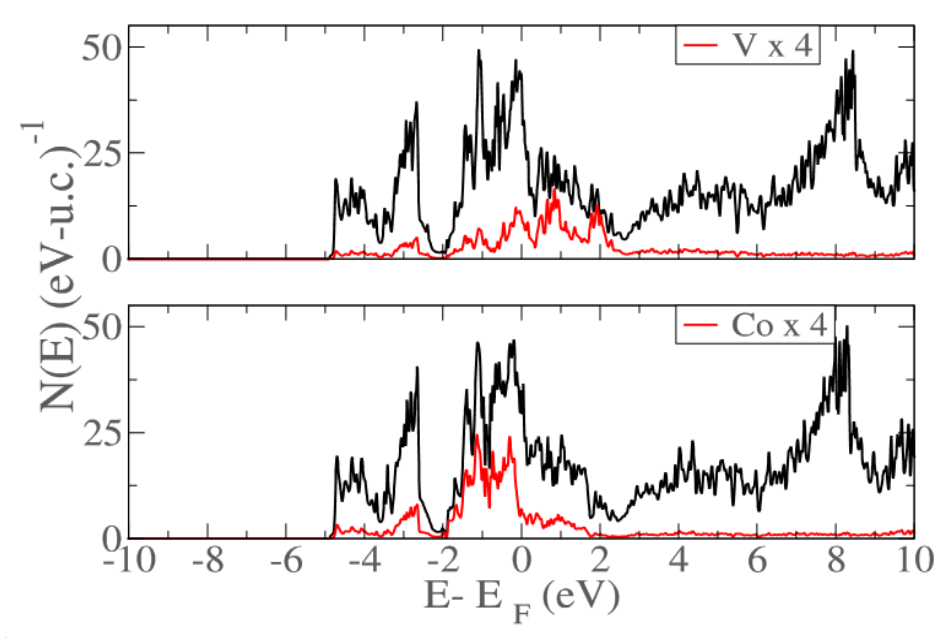


FIGURE S3. Calculated DOS for cobalt versus vanadium dopants into BaFe₂As₂. The DOS of the dopants is multiplied by 4 for clarity.

[S1] A. S. Sefat, Current Opinion Solid State Mater. Sci. 17, 59 (2013).

[S2] H. Xiao, T. Hu, A.P. Dioguardi, N. Roberts-Warren, A.C. Shockley, J. Crocker, D.M. Nisson, Z. Viskadourakis, X. Tee, I. Radulov, C. C. Almasan, N. J. Curro, and C. Panagopoulos, Phys. Rev. B **85**, 024530 (2012).

[S3] J. Knolle, I. Eremin, A. Akbari, and R. Moessner, Phys. Rev. Lett. 104, 257001 (2010).

[S4] D. K. Singh, and P. Majumdar, Phys. Rev. B 96, 235111 (2017).

[S5] L. Li, H. Cao, D. S. Parker, S. J. Kuhn, and A. S. Sefat, Phys. Rev. B 94, 134510 (2016).

[S6] A. S. Sefat, L. Li, H. Cao, M. A. McGuire, B. C. Sales, R. Custelcean, and D. S. Parker, Sci. Rep. 6, 21660 (2016).

[S7] I. I. Mazin, M. D. Johannes, L. Boeri, K. Koepernik, and D. J. Singh, Phys. Rev. B 78, 085104 (2008).